Spontaneous emission rates of dipoles in photonic crystal membranes

A. Femius Koenderink

Laboratory of Physical Chemistry, Swiss Federal Institute of Technology (ETH), 8093 Zürich, Switzerland

Maria Kafesaki

Institute of Electronic Structure and Laser (IESL), Foundation for Research and Technology Hellas (FORTH), P.O. Box 1527, 71110 Heraklion, Crete, Greece, and
Department of Materials Science and Technology, University of Crete, Greece

Costas M. Soukoulis

Ames Laboratory, Iowa State University, Ames, Iowa 50011, and
Institute of Electronic Structure and Laser (IESL), Foundation for Research and Technology Hellas (FORTH), P.O. Box 1527, 71110 Heraklion, Crete, Greece, and
Department of Materials Science and Technology, University of Crete, Greece

Vahid Sandoghdar

Laboratory of Physical Chemistry, Swiss Federal Institute of Technology (ETH), 8093 Zürich, Switzerland

Received December 6, 2005; accepted January 20, 2006; posted February 6, 2006 (Doc. ID 66493)

We show theoretically that two-dimensional (2D) photonic crystals in semiconductor membranes strongly modify the radiative decay of dipole emitters. Three-dimensional finite-difference time-domain calculations show over 7 times inhibition and 15 times enhancement of the emission rate compared with vacuum for judiciously oriented and positioned dipoles. Emission rate modifications inside the membrane mimic the local mode density in a simple 2D model. The inhibition of emission saturates with crystal size around the source, with a $1/e$ size that scales as the inverse gap bandwidth. Owing to the vertically guided mode structure, inhibition occurs only near the slab center, but enhanced emission persists also outside the membrane. We find that emission changes can even be observed in experiments with ensembles of randomly oriented dipoles. © 2006 Optical Society of America

OCIS codes: 130.130, 160.0160, 180.5810, 270.5580.

1. INTRODUCTION

The past decade has seen a remarkable increase in experimental efforts to control spontaneous emission dynamics of dipole transitions by tailoring the dielectric surroundings of the source. Although studies in elementary geometries, such as planar interfaces[1–6] or spherical particles,[7–10] remain of current interest, particular impetus in spontaneous emission control derives from solid-state cavity quantum electrodynamics (CQED)[6,11] and the increasing capability to shape semiconductors on the nanometer scale. Of particular interest in this respect are photonic bandgap materials.[12] As first proposed by Bykov[13] and Yablonovitch,[14] three-dimensionally periodic arrangements of dielectric material on wavelength-sized scales allow to create a medium in which spontaneous emission processes can not only be enhanced but also completely inhibited. These photonic crystals offer many exciting prospects in fundamental physics, ranging from CQED, control of blackbody radiation[15], and the slowing and storage of light,[16] as well as device opportunities[12] for producing and processing of optical signals on submicrometer length scales.

Although efforts in realizing spontaneous emission control in three-dimensional (3D) photonic bandgap crystals have been partly successful,[17–19] the advantages of easier fabrication and characterization have motivated many groups to work on lower-dimensional, i.e., two-dimensional (2D) crystal structures. Photonic crystals in thin semiconductor membranes have recently shown particular promise to realize ultrasmall cavities with very high quality factors, suited for quantum optics in the strong coupling limit.[20–22] In addition, the first experimental evidence[23–25] for large emission inhibition of quantum dots and quantum wells in photonic crystal membranes was recently reported. Although all these results suggest that the effect of the gap in the in-plane band structure is greatly enhanced by the vertical index contrast, a systematic study of the potential for spontaneous emission rate control offered by membrane photonic crystals is lacking.

In this paper we present a theoretical study of the spontaneous emission rate modifications in membrane photonic crystals that consist of only a finite number of unit cells. Such an analysis is particularly challenging for

 © 2006 Optical Society of America

structures that are limited in size, because approaches that are based on the commonly used plane-wave electromagnetic eigenfunction calculations[26–31] cannot be used. We have therefore used a method similar to that recently proposed by Hwang *et al.*,[32] Xu *et al.*[33,34], and Hermann and Hess,[35] based on the 3D finite-difference time-domain method (FDTD).[36]

The paper is organized as follows. In Section 2 we summarize our theoretical approach and discuss the numerical characteristics of the method. In Section 3 we discuss the spontaneous emission lifetime modification for a dipole in the center of a photonic crystal membrane and compare our result with both 2D and 3D plane-wave calculations of the local density of states. In Section 4 we focus on the dependence of the emission lifetime on the orientation of the transition dipole moment and the position of the emitter in the central plane of the membrane. In Section 5 we consider the role of the crystal size in determining the spontaneous emission rate and propose a relation between the width of the emission gap and the number of crystal rows that need to surround the emitter to obtain maximum inhibition. In Section 6, we focus on the effect of membrane thickness and of the height of the dipole above the membrane center on the emission lifetime. We show that a simple model for the emission rate in homogeneous dielectric slabs explains many of the observed features. Finally, in Section 7 we discuss the prospects for experiments involving localized ensembles of emitters with randomly distributed dipole moments. Conclusions are presented in Section 8.

2. METHOD

The quantum analysis of spontaneous emission based on Fermi's Golden Rule asserts that the spontaneous emission rate of an emitting dipole varies with its position $\mathbf{r}$ and orientation $\hat{\mathbf{d}}$, depending on the availability of photon modes at the source position and frequency ω. The central quantity that takes this into account is the local radiative density of states[37] (LRDOS) $\rho(\mathbf{r},\hat{\mathbf{d}},\omega)$. The LRDOS is a classical electromagnetic quantity that appears in the classical analysis of radiating antennas, where it describes the power needed to drive a pointlike electric dipole oscillating at a fixed current.[32–35] This power is due to the work $W \propto \mathbf{j}\cdot\mathbf{E}$ that the field $\mathbf{E}$ radiated by the source $\mathbf{j}(\mathbf{r},t)$ does on the source itself. The rate of spontaneous emission Γ in a dielectric structure, normalized to the free-space rate Γ_{vac}, can therefore be found by comparing the work W done on the source in the dielectric structure to the work W_{vac} done on the same current source in vacuum.

We use the 3D FDTD method for our calculations throughout this work. An important advantage of the FDTD method[33–36] over conventional methods[2,28,29] to calculate the LRDOS is that the field $\mathbf{E}$ of a point source, and hence the LRDOS, is readily calculated without solving for the electromagnetic eigenmode basis of the dielectric structure. Furthermore, the FDTD method can even be used to calculate the LRDOS for lossy systems in which eigenmode expansions are invalid. In this paper we follow the method of Hermann and Hess,[35] in which the LRDOS is simulated for a wide frequency range at once via broadband temporal excitation of a dipole point source. For a pulsed source with frequency spectrum $\mathbf{j}(\mathbf{r}_0,\omega)$, the time trace of the electric field $\mathbf{E}(\mathbf{r}_0,t)$ at the position $\mathbf{r}_0$ of the source can be Fourier transformed to determine the LRDOS in terms of its vacuum value $\rho_{\mathrm{vac}}(\omega)$:

$$\rho(\mathbf{r}_0,\hat{\mathbf{d}},\omega) = \rho_{\mathrm{vac}}(\omega)\frac{W(\mathbf{r}_0,\hat{\mathbf{d}})}{W_{\mathrm{vac}}} = \rho_{\mathrm{vac}}(\omega)\frac{\mathbf{j}(\mathbf{r}_0,\omega)\cdot\mathbf{E}(\mathbf{r}_0,\omega)}{\mathbf{j}(\mathbf{r}_0,\omega)\cdot\mathbf{E}_{\mathrm{vac}}(\mathbf{r}_0,\omega)}. \tag{1}$$

We have evaluated the validity and pitfalls of this numerical method by comparing the simulated spontaneous emission rate enhancement with exact analytical results for a dipole in a dielectric sphere,[7–9,35] and for a dipole near a planar interface between two dielectrics.[2–4] Figure 1 shows that accurate results for the emission rate modification are obtained by the FDTD method for a representative test case in which a dipole is placed near a planar interface between air and silicon. By examining the LRDOS obtained with pulses at different center frequencies, we have established that results consistent to within $\sim$1% can be obtained in the frequency ranges in which the vacuum emission power of the dipole current pulse exceeds $\sim$5% of its maximum value. Throughout this paper we use temporal excitation pulses with a Gaussian envelope and bandwidths around 50% of the central frequency.

Agreement of the simulated LRDOS with the exact LRDOS depends not only on sufficient spectral overlap of the input current with the frequency range of interest but also on the spatial discretization. Apart from the obvious requirement that the discretization must be sufficiently

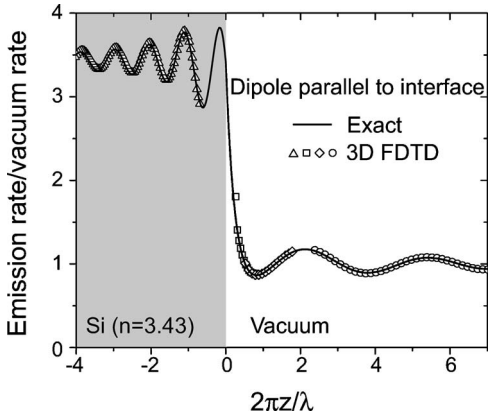

Fig. 1. Symbols, spontaneous emission rate normalized to emission rate in vacuum as a function of normalized frequency for a dipole in front of and oriented parallel to a planar dielectric interface separating silicon (ϵ=11.76) and vacuum calculated using the 3D FDTD method. The normalized frequency corresponds to the separation z between source and interface, normalized to the vacuum emission wavelength λ. For the dipole in vacuum (positive z), results are shown for three separations. In units of the grid discretization Δ, these are $z=25\Delta$ (circles), 5Δ (diamonds), and 2Δ (squares). The same temporal excitation pulses were used for $z=25\Delta$ and 5Δ to span two different normalized frequency ranges $2\pi z/\lambda$. For the dipole in silicon (negative z), the results shown were obtained with a single excitation pulse and a single dipole position at $z=-25\Delta$ from the interface. Excellent agreement with the exact local radiative density of states modification (solid curve) is obtained. The total simulation volume was $300\times300\times120\Delta^3$ in size.

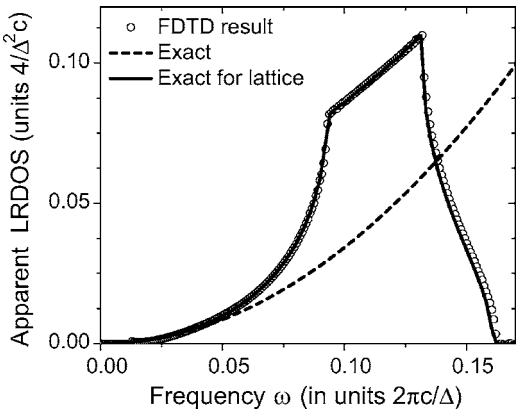

Fig. 2. Symbols, FDTD approximation to the LRDOS of a *homogeneous* medium ($\epsilon=11.76$) obtained using the FDTD method and Eq. (1), taking a very broadband temporal excitation of the source dipole. The dashed parabola indicates the exact LRDOS. Agreement to within 5% is obtained only for frequencies $\omega < 0.03(2\pi c)/\Delta$, for which the wavelength in the highest-index medium remains longer than 10 times the discretization grid spacing Δ. Deviations are due to the unphysical dispersion relation on the grid [Eq. (2)] and the wave vector cut-off of the grid at $k=(\pi/\Delta,\pi/\Delta,\pi/\Delta)$, as evident from the excellent agreement of the FDTD result with the exact *grid* density of states per volume obtained by integrating Eq. (2).

fine to resolve features of the dielectric structure, the accuracy is affected by the dispersive properties of the cubic discretization grid itself. To illustrate this point, Fig. 2 shows the apparent LRDOS of a homogeneous dielectric of index $n=3.4$ over a very wide frequency range, obtained by the procedure described in Eq. (1). The exact LRDOS of the homogeneous dielectric (parabola in Fig. 2) equals n times the vacuum LRDOS, independent of frequency. Figure 2 shows that large discrepancies occur for large frequencies. The deviation exceeds 5% for frequencies at which the wavelength in the dielectric is shorter than 10Δ, where Δ is the spacing between adjacent discretization grid points. The source of the discrepancy is the well-known anisotropic dispersion of the cubic grid as well as the cut-off of the grid for wave vectors in excess of $(\pi/\Delta,\pi/\Delta,\pi/\Delta)$. We have calculated the density of states of the discretization grid (filled with vacuum and with medium of index n) from its dispersion relation,[36]

$$\sin\left(\frac{\omega\Delta t}{2}\right)^2=\frac{c\Delta t}{n\Delta x}\left[\sin\left(\frac{k_x\Delta}{2}\right)^2+\sin\left(\frac{k_y\Delta}{2}\right)^2+\sin\left(\frac{k_z\Delta}{2}\right)^2\right], \tag{2}$$

where Δt is the magnitude of the time step, Δ is the grid spacing, and c is the speed of light in vacuum. The excellent agreement of the grid density of states with the apparent LRDOS calculated by the FDTD method for a dipole in a homogeneous dielectric in Fig. 2, confirms the role of the density of states of the numerical discretization grid in spontaneous emission rate calculations. We conclude that an accuracy better than $\sim 5\%$ for spontaneous emission rates calculated by the FDTD method, requires discretization grids with over 10 grid points per wavelength at the frequency of interest in the highest index medium.

Finally, we note that accurate results require that the Fourier transforms of $\mathbf{j}(\mathbf{r}_0,t)$ and $\mathbf{E}(\mathbf{r}_0,t)$ be calculated without zero padding of the time series, as done by many fast Fourier transform routines that use arrays of length equal to a power of 2. To find the power spectrum radiated by the dipole, the complex Fourier transforms F of the real-time series of $\mathbf{j}$ and $\mathbf{E}$ are combined according to

$$\mathbf{j}(\mathbf{r}_0,\omega)\cdot\mathbf{E}(\mathbf{r}_0,\omega)=\mathrm{Re}[F\mathbf{j}]\cdot\mathrm{Re}[F\mathbf{E}]+\mathrm{Im}[F\mathbf{j}]\cdot\mathrm{Im}[F\mathbf{E}]. \tag{3}$$

The two terms are nearly equal in magnitude but opposite in sign. The desired sum is approximately 10^4 times smaller than either term. Even if time stepping is continued until the fields have decayed by several orders of magnitude, zero padding introduces noise that is small compared to either term in Eq. (3) but sizeable compared with the signal that remains after summing them. Furthermore, strongly resonant features in LRDOS spectra need to be handled with care. Time series of field and current are typically limited to total time spans of only 10^2—10^3 optical cycles, as the 3D FDTD method is very computationally intensive. For resonances with quality factors in excess of $\sim 10^2$, time series are truncated before the fields have fully decayed, giving rise to artifacts in the Fourier transform that can fully dominate the simulated LRDOS spectra. To remove such artifacts, we have used a seventh-order Daubechies apodization filter.[38] We have checked the validity of this approach for FDTD simulations of a single-mode high-Q photonic crystal cavity,[39] which has a much narrower resonance in the LRDOS than appears in any of the results presented below. For such a single-mode system, the time series of the field can be extrapolated to obtain the true LRDOS from an untruncated time series.

3. COMPARISON WITH 2D AND 3D LRDOS FOR VERTICALLY INFINITE CRYSTALS

We consider spontaneous emission rate modifications in 2D photonic crystals within semiconductor membranes, as studied for the dipole-position averaged case by Lee and Yariv.[34] We focus on finite structures consisting of membranes with dielectric constant $\epsilon=11.76$ and thickness 250 nm perforated with a hexagonal lattice of holes (lattice spacing $a=420$ nm) of radius $0.3a$. Such membranes have a wide bandgap for TE guided modes, i.e., modes with electric field in the central plane of the slab pointing along the membrane, but no gap for TM modes. The geometrical parameters are typical for the membrane structures in which high Q factor cavities for strong coupling CQED were recently realized[20–22] and for which first evidence of inhibition of spontaneous emission was recently presented.[23,24] We simulate finite crystallites of hexagonal shape and various sizes ranging from 1 to 12 lattice spacings in radius, as counted from the central hole (see Fig. 3). The crystals were terminated by either semiconductor or air extending into the Liao absorbing boundary conditions. We have used 14 or 20 grid points per lattice constant, with a doubled grid density in the vertical direction. To reduce staircasing errors due to the discretization of the structure, we used volume averaging

of the dielectric constant in each grid cell.[40] In the simulations, membranes were surrounded above and below by up to 1 μm of air.

First, we consider the spontaneous emission lifetime for a dipole that is located in the middle of the central air hole of a structure of $L=6$ lattice spacings across. Figure 4 shows the LRDOS normalized to the vacuum LRDOS for an in-plane oriented dipole that points along the x axis (see Fig. 3), i.e., from air hole to air hole. For dipole orientations in the plane of the slab, the spontaneous emission rate is strongly modulated as a function of normalized frequency a/λ (where λ is the vacuum wavelength). We find a frequency range from $a/\lambda=0.25$ to $a/\lambda=0.33$ of inhibition of the emission rate that overlaps with the in-plane photonic bandgap for the TE modes guided by the membrane, as was also observed in calculations by Lee *et al.*[34] An inhibition of the LRDOS by a factor $\gtrsim 7$ compared with vacuum is obtained. This value translates to over 30 times inhibition as compared to the emission modification at frequencies far below the bandgap at the same position. Above and below the range for which the emission is strongly reduced, which we will call the *emission gap*, the emission rate is strongly modulated, featuring enhancements of the emission rate by factors up to 20 times compared with vacuum, or over 5 times compared with the LRDOS in the long wavelength limit at the same position. As will be discussed below, the fringes outside the emission gap are due to Fabry–Perot oscillations caused by the finite lateral size of the crystal.

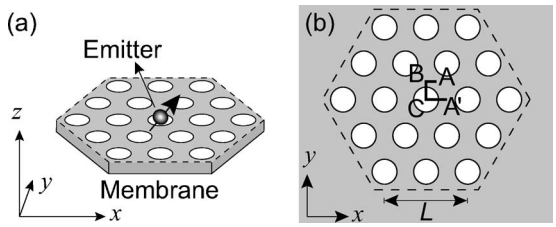

Fig. 3. (a) Schematics of the geometry for calculating the spontaneous emission rate modification in membranes. We consider dipoles near the center of 2D finite photonic crystals, consisting of a hexagonal array of air holes (lattice spacing a, radius r) in a semiconductor membrane (thickness d). The position and orientation of the emission dipole are specified along Cartesian axes, where z specifies the height above the center of the membrane and x and y are in the plane of the membrane. (b) (top view) The finite crystallites are hexagonally truncated such that the central air hole is surrounded by the same number of holes [indicated by the crystallite radius L ($L=2a$ in the sketch)] in all directions. Outside the truncation boundary (dotted hexagon), the membrane was terminated by either semiconductor or air. For Fig. 5, the dipole position was scanned over the trajectory from point A via B, C to A'.

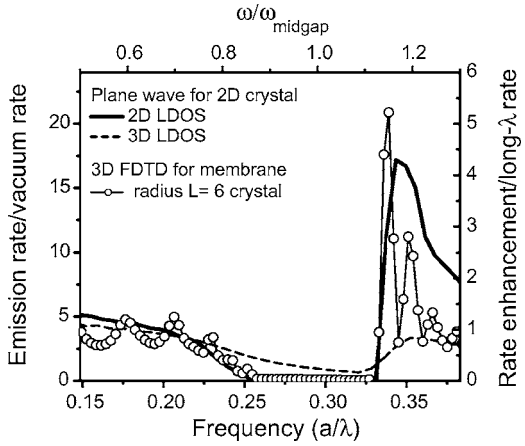

Fig. 4. Connected open symbols, modification of the radiative emission rate compared with vacuum (refer to left axis) versus normalized frequency a/λ (refer to bottom axis). This result is calculated with the 3D FDTD method for a dipole in the central air hole of a crystal of radius $L=6a$ with $r/a=0.3$, $a=420$ nm in a semiconductor membrane [$\epsilon=11.76$, $d=250$ nm (truncated by semiconductor)], oriented along the x axis in Fig. 3, in the plane of the membrane. In the apparent gap, emission is reduced to about 0.14 times the vacuum emission rate. Refer to the top and right-hand axes for frequency normalized to the midgap frequency, and emission rate enhancement normalized to the emission rate modification at the same position for frequencies far below the gap. Solid curve (refer to top and right-hand axis), modification of the 2D LRDOS in an infinite crystal (also $r/a=0.3$, $\epsilon=11.76$) in the center of an air hole, according to the plane wave-method. Dashed curve, modification of the 3D LRDOS in an infinite 2D crystal (again $r/a=0.3$, $\epsilon=11.76$) that extends infinitely in the vertical direction, calculated with the plane-wave method. The LRDOS modification in the center of the membrane is much stronger than the weak LRDOS modification in the vertically unconfined crystal.

It is perhaps surprising that significant control over spontaneous emission dynamics is possible for selected dipole positions and orientations, despite the fact that no full bandgap exists. It appears that the large vertical index contrast greatly enhances the effect of the in-plane periodicity on spontaneous emission. To confirm this notion, we have used the H-field inverted-matrix plane-wave expansion method to calculate the local radiative density of states in infinite 2D photonic crystals that are not confined vertically.[26,28,29] In addition to the 3D LRDOS, we have also calculated the 2D LRDOS, which counts only modes that propagate in the plane of periodicity. For the 2D (3D) case, we used 8100 (84000) nonequivalent k points,[41,42] which were distributed over half of the full Brillouin zone to avoid erroneous results[28] owing to the reduced symmetry of the polarization-resolved LRDOS.[31] We have scaled both the frequency axis and the vertical axis to optimally overlap the resulting 2D and 3D LRDOS (normalized by the 2D respectively 3D vacuum LRDOS) for an x-oriented dipole in the center of an air hole with the LRDOS in the membrane (see Fig. 4). Naturally, the 2D (local) density of states of the 2D crystal shows a full gap for dipole orientations in the plane of periodicity, corresponding to the TE bandgap in the 2D band structure. The gap is accompanied by characteristic emission enhancement at the gap edges owing to low group-velocity modes.[28] For a dipole at the center of an air hole, this enhancement occurs at the high-frequency edge of the gap, as is also apparent in the membrane. In stark contrast, the 3D LRDOS is only weakly modulated for vertically infinite crystals, owing to the contributions of modes with wave vector components along the air cylinders.[43,44] Although the 2D bandgap causes a shallow minimum in the 3D LRDOS for a dipole in the center of an air hole, the bandwidth of emission inhibition is much narrower than the bandwidth of the 2D bandgap, and no sign of emission enhancement at the bandgap edges remains.[28,44] The comparison of plane-wave calculations with the FDTD result shows that the vertical confinement

offered by membranes prevents the washing out of the characteristic features of the 2D LRDOS that occurs for vertically unconfined crystals. First, the emission gap in the membrane referenced to the long wavelength LRDOS at the same position in the crystal amounts to an inhibition by a factor around 30, which is over five times stronger than the inhibition obtained if the structure is not truncated in the vertical direction. Second, the relative inhibition gap bandwidth of 24% offered by the membrane structure is close to the bandwidth of 25% in the 2D band structure. Third, we note that the emission-rate enhancement at the blue edge of the gap is retrieved in the membrane structure. The enhancement of ~6 times compared with the emission rate in the long wavelength limit is in good agreement with the enhancement observed in the 2D LRDOS. This is especially surprising when the finite size of the crystal and the effect of its truncation on the exact spectral position and quality factor of the Fabry–Perot oscillations are considered.

4. DEPENDENCE ON POLARIZATION AND LATERAL POSITION

To obtain a more complete overview of the spontaneous emission control offered by membranes, we consider the LRDOS modification for different positions in the central unit cell of a crystallite that is again $6a$ in radius, terminated on the sides by semiconductor material. Figure 5 shows contour plots of the LRDOS normalized to the vacuum LRDOS as a function of frequency in the range of the TE bandgap, for dipoles that are vertically centered in the membrane and positioned along the path indicated in Fig. 3(b). This trajectory spans the boundary of the irreducible part of the real space 2D unit cell and ensures that the Cartesian dipole orientations in Fig. 5 are always parallel or perpendicular to the trajectory. Figure 5 confirms the occurrence of a deep gap in the spontaneous emission rate for dipole orientations in the plane of the membrane for all positions close to the center of the crystal. Moreover, we find that there is no gap in the emission rate for dipoles oriented perpendicular to the membrane but only a weak dependence on frequency, as expected from the absence of a 2D bandgap for the TM-guided modes of the membrane.

A detailed inspection of Fig. 5 shows furthermore that strong emission enhancement at the blue edge of the emission gap is predicted to occur only for dipoles positioned inside the air hole. In contrast, emission enhancement at the red edge of the gap is predicted only for dipoles located outside the air hole, and preferentially for dipoles oriented perpendicular to the air-hole edges. This difference between dipole positions inside and outside the air holes is confirmed by the 2D LRDOS modification predicted by the plane-wave method (Fig. 6) and is consistent with the well-known difference in spatial distribution of the low group-velocity modes that cause the spontaneous emission enhancement. These modes are preferentially concentrated in the air (dielectric) region for the high (low) frequency edge of the gap. Disregarding the Fabry–Perot oscillations owing to the finite crystal size, we find that the spectral and spatial location of the enhancements, the relative magnitude of the enhancements compared with the LRDOS modifications for frequencies far below the gap, and the bandwidth of the gap in Figs. 5(a) and 5(b) are in good qualitative agreement with the 2D LRDOS modification calculated by the plane-wave method (Fig. 6). It should be noted that good agreement is limited to dipole orientations parallel to the membrane, as the vertical confinement in the membrane causes a much larger shift to higher frequencies for the photonic band structure for TM polarization than for TE polarization.[45] The results in Fig. 5 do not agree for any polarization with the much weaker 3D LRDOS modification for a crystal that is infinitely extended in the vertical direction.

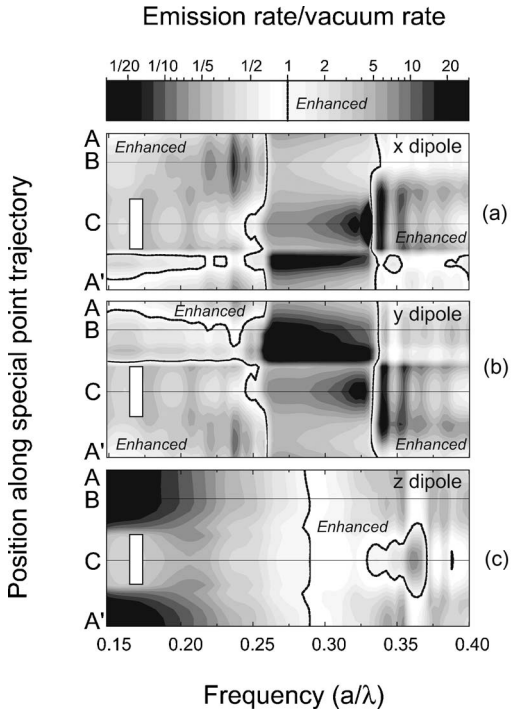

Fig. 5. Contour plot of the LRDOS normalized to the vacuum LRDOS calculated by 3D FDTD as a function of frequency and as a function of position along the trajectory in Fig. 3 for dipoles in a finite membrane crystallite of radius $L=6a$. Panels (a)–(c) refer to the three orthogonal dipole orientations along the respective x, y, and z axes. Vertically, the dipoles are placed in the middle of the membrane ($z=0$). In-plane dipole orientations show a large emission gap for $0.25<\omega<0.33$ for all positions, while no gap occurs for the vertically oriented dipole. Enhancement of the emission rate for horizontally oriented dipoles occurs on the high-frequency edge when the dipole is located in air (positions indicated by the vertical white bars in all panels) and on the low-frequency edge when the dipole is located in dielectric. The gray-scale (indicated on top) is logarithmic both for inhibition and enhancement (regions separated by contour line at unity, and labeled as 'Enhanced' as appropriate).

5. EMISSION-GAP WIDTH AND THE CRYSTAL SIZE REQUIRED FOR MAXIMUM EMISSION-GAP DEPTH

Figures 4 and 5 allow us to conclude that large changes in spontaneous emission rate occur for properly oriented dipoles located near the center of small crystals in semiconductor membranes. In this section we investigate how large the crystal around the dipole must be to obtain a

significant emission gap. In Fig. 7 the spontaneous emission modification is shown for a horizontally x-oriented dipole in the central air holes of semiconductor-truncated crystals of various sizes. The most striking features in Fig. 7 are the deepening of the emission gap with increasing size of the crystallite around the source, the steepening of the emission-gap band edges, and the decrease of the frequency spacing between modulations of the emission rate outside the emission gap. The decreasing frequency spacing between these fringes with increasing crystal size validates their interpretation as Fabry–Perot type resonances caused by the impedance mismatch occurring at the outer edges of the crystal. When crystals are truncated by air rather than by semiconductor, the oscillations change in amplitude and shift in frequency at unchanged frequency spacing between fringes, as consistent with an interpretation as Fabry–Perot resonances. Unlike the Fabry–Perot oscillations that occur for transmission through finite crystals,[46,47] however, the oscillations in the LRDOS depend on *all* size-dependent resonances in the system instead of solely those with specific wave vectors. Independently of the size and nature of the truncation, the LRDOS at the high-frequency edge of the emission gap exceeds 15 times the vacuum LRDOS, corresponding to an enhancement of at least 5 times compared with the emission rate typically observed below the gap in the range $0.15 \leqslant a/\lambda \leqslant 0.22$.

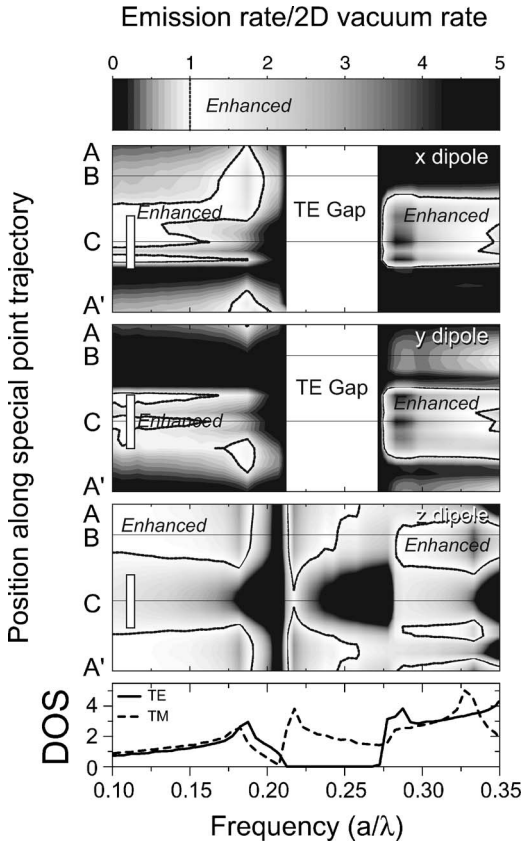

Fig. 6. Top three panels, contour plots of the 2D LRDOS normalized to the vacuum 2D LRDOS according to the plane-wave method for a dipole in a 2D photonic crystal (air holes $r/a=0.30$ in a matrix of $\epsilon=11.76$) as a function of emission frequency (horizontal axis) and position of the dipole along the trajectory indicated in Fig. 3 for three perpendicular dipole orientations as indicated. White bars indicate the extent of the trajectory inside air. For in-plane oriented dipoles (top two panels), the 2D LRDOS shows a full gap (labelled as TE gap). The bottom panel shows the 2D TE and TM total density of states per area in units $a^{-1}c^{-1}$.

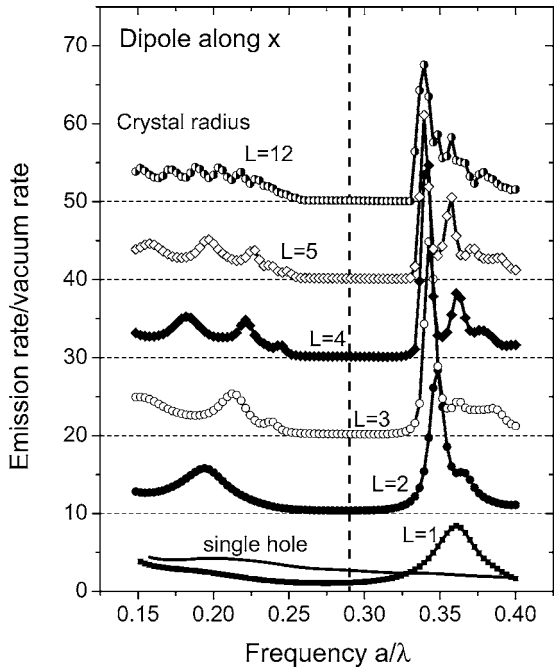

Fig. 7. Lines with symbols, LRDOS normalized to vacuum LRDOS versus frequency, depending on crystallite size (crystal radii $L=1$ to 12 as indicated, curves shifted vertically, and different symbols as labelled) for an x-oriented dipole in the central air hole of hexagonal crystallites (truncated with semiconductor). With increasing number of layers, the gap deepens, the gap edges become steeper, and the spacing decreases for the Fabry–Perot fringes that occur for frequencies below the gap $a/\lambda<0.25$ and above the gap $a/\lambda>0.32$. For a single air hole in a semiconductor (curve, no symbols) no gap or resonance is observed, while for a single crystal layer (small dots) a resonance at frequencies above the gap is already evident. The vertical dashed line marks the midgap frequency for which the inhibition is reported in Fig. 8.

The value of the LRDOS for frequencies within the emission gap saturates with increasing crystal size. In Fig. 8, we plot the emission inhibition gap minimum for the frequency $a/\lambda=0.29$ in the middle of the emission gap as a function of crystal radius. The LRDOS in the middle of the gap decreases exponentially[35,43,48] to its limiting value of 0.14 times the vacuum value, with a $1/e$ crystal radius of just $L_{\mathrm{gap}}=0.7a$. It is remarkable that only so few crystal layers are needed to create the emission gap. This observation suggests that the emission gap can be expected to be very robust against fabrication disorder. The $1/e$ radius for the emission gap can be compared with the number of layers needed for a cavity to reach its ultimate quality factor. The inverse quality factor of low-volume microcavities in 2D photonic crystals approaches its limiting value set by the out-of-plane losses in an exponential manner as the number of crystal rows surrounding the cavity is increased.[45,49] For unoptimized and optimized single-hole cavities[21,39,45] operating at frequencies in the middle of the bandgap, the same characteristic length of $0.7a$ is found for the inverse quality factor.

Figure 8 also shows the gap minimum as a function of crystal size for photonic crystal membranes of different

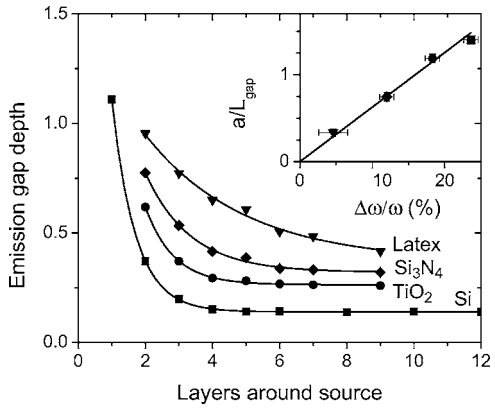

Fig. 8. Solid squares, spontaneous emission rate compared with vacuum for the midgap frequency labeled in Fig. 7 versus crystallite radius. Circles, diamonds, and triangles, emission-gap depth in the middle of the emission gap for membranes (thickness 250 nm, $a=250$ nm, $r/a=0.3$) of TiO_2 ($\epsilon=6.25$), Si_3N_4 ($\epsilon=4$), and latex ($\epsilon=2.25$). Curves are exponential fits to the points. The inset shows the inverse fitted exponential decay lengths (symbols, in units of a) versus the relative bandwidth of the emission gap. The line corresponds to $a/L_{\mathrm{gap}}=2\pi\Delta\omega/\omega$.

dielectric constants $\epsilon=6.25$ (titanium dioxide, $a=250$ nm), $\epsilon=4.0$ (silicon nitride, $a=250$ nm) and $\epsilon=2.55$ (polystyrene, $a=250$ nm). As expected, the maximum achievable inhibition decreases with reduced index contrast, and the characteristic number of layers L_{gap} needed to achieve the inhibition increases with decreasing refractive index contrast. The inset in Fig. 8 shows the inverse characteristic length L_{gap} as a function of the relative band width $\Delta\omega/\omega$ of the emission gap. We observe that L_{gap} is inversely proportional to the width of the bandgap. This inverse dependence is well known for the penetration depth of light in dielectric mirrors and for simple two-band models of Bragg diffraction from photonic crystal lattice planes.[46] In such a model the field intensity decays exponentially into the crystal, with intensity decay length $D/(\pi\Delta\omega/\omega)$, where D is the separation between lattice planes. The same behavior is found for L_{gap}, as shown by quantitative comparison of L_{gap} taken from the FDTD simulations with $a/(2\pi\Delta\omega/\omega)$. This observation highlights the universal role of the gap width as a measure for the interaction strength of the photonic structure with light, as proposed in Refs. 48 and 50. A more thorough investigation of this hypothesis should include calculations for 2D and 3D photonic crystal geometries and is outside the scope of this paper.

6. DIFFERENT CONTRIBUTIONS TO THE EMISSION RATE DERIVED FROM A SIMPLE HOMOGENEOUS SLAB MODEL

Figure 8 shows not only that the emission gap in membrane photonic crystals deepens exponentially with lateral crystal size but also that the inhibition that is ultimately achieved for sufficiently large crystals depends on the membrane index. Similarly, we expect the emission-gap depth to depend on the thickness of the membrane. We have calculated the spontaneous emission rate for a dipole in the central air hole of photonic crystal membranes as considered in Fig. 4 ($a=420$ nm, $r/a=0.3, \epsilon=11.76, L=6$) for membrane thicknesses between 50 and 800 nm. Figure 9 shows the emission rate normalized to the vacuum rate at the center frequency of the emission gap, which shifts from $a/\lambda=0.45$ at $d=50$ nm to lower frequencies as the membrane thickness increases. The center frequency of the gap saturates at around $a/\lambda=0.26$ for thicknesses around 400 nm. For membrane thicknesses above 600 nm contributions of higher-order slab-guided modes compromise the definition of the gap edges that allows us to find the center frequency. For these thicknesses the Fabry–Perot oscillations for frequencies just below the red edge of the gap merge with Fabry–Perot oscillations for in-gap frequencies. The enhancement at the blue edge of the gap remains clearly visible and remains above 10 times the vacuum LRDOS. For thicknesses above 700 nm the emission-rate modulation in the frequency range around the gap approaches an asymmetric sawtoothlike shape, similar to the 3D LRDOS in a vertically infinite crystal (Fig. 4).

Figure 9 shows that significant inhibition of emission occurs for membrane thicknesses below 400 nm, with an optimum thickness for inhibition around 250 nm. For larger thicknesses, the emission rate is significantly less inhibited, and even enhanced for $d \geqslant 600$ nm. As a simple model to explain the thickness dependence of the emission rate, we consider the emission rate of dipoles in homogeneous dielectric slabs. We have used the approach of Urbach and Rikken[51], which allows us to separate the contributions to the LRDOS of modes that propagate outside the dielectric slab from the contributions of the slab-guided modes to the lifetime of in-plane oriented dipoles. In a high-index dielectric slab, such as a silicon membrane in air (Fig. 9, inset) the LRDOS contribution of propagating modes is strongly reduced to only ~0.08 times the vacuum LRDOS. However, the LRDOS contri-

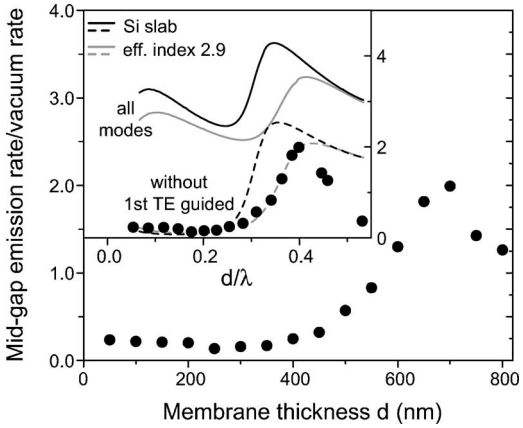

Fig. 9. Solid circles, emission rate normalized to the vacuum rate at the center frequency of the emission gap for an x-oriented dipole in the center of a photonic crystal membrane as a function of membrane thickness d. For membranes above 500 nm thickness (around one-third of the emission wavelength), no inhibition of emission remains. Inset, (symbols) the same data plotted as a function of thickness normalized to the gap center wavelength (which shifts with thickness). Solid curves, LRDOS for an in-plane oriented dipole in the center of a homogeneous membrane of refractive index 3.45 (black) and of index 2.9 (gray). Dashed curves, same as solid curve but without the contribution of the first TE-polarized slab guided mode that is suppressed by the 2D photonic bandgap.

bution of the guided modes causes the overall LRDOS, and hence the spontaneous emission rate for an embedded dipole to exceed the vacuum LRDOS significantly.

For a photonic crystal membrane that has a full bandgap for the first TE slab-guided mode, one expects the LRDOS contribution of the first TE guided mode to vanish completely. To assess the validity of this hypothesis, we plot the midgap emission rate in Fig. 9 as a function of normalized thickness d/λ in the inset of Fig. 9 and compare it with the LRDOS in a homogeneous silicon slab, *without* the contribution of the first TE guided mode. The comparison reveals that the emission rate in the emission gap of Si photonic crystal membranes indeed follows qualitatively the same dependence on slab thickness as the LRDOS in a homogeneous silicon membrane without the contribution of the first TE guided mode, yet shifts toward larger thicknesses. The sharp increase of the emission rate with thickness around $d/\lambda=0.3$ allows us to fit an effective refractive index of $n_{\mathrm{eff}}\sim 2.9$ for which the LRDOS at gap frequencies of the membranes most resembles the LRDOS without the first TE guided mode contribution in unpatterned dielectric slabs. This value is higher than the effective index of ~2.8 derived from the volume-averaged dielectric constant of the membrane. It is important to note, however, that the sharp increase of the emission rate is due to the combined contributions of the second-order TM and the third-order TE slab guided mode, for which the derivation of an effective index is highly nontrivial.

The interpretation of lifetimes in photonic crystal membranes in terms of the propagating and guided mode LRDOS contributions in a dielectric slab is also relevant for the dependence of the LRDOS on the separation of the dipole from the center of the photonic crystal membrane. In Fig. 10 we plot the emission rate at two key frequencies for an x-oriented dipole in the central air hole of a membrane of 250 nm thickness that is shifted vertically above the center of the slab. For a frequency $a/\lambda=0.28$ in the emission gap [Fig. 10(a)] we find that the inhibition of emission quickly vanishes as the dipole is moved away from the center of the slab. No traces of inhibition remain for dipoles that are further than ~100 nm away from the slab center. In contrast, we find that the enhancement at $a/\lambda=0.33$ at the blue edge of the gap is not restricted to dipole positions within 100 nm of the slab center. Emission enhancement by a factor of 5 persists even 50 nm above the slab, as we proposed recently.[52]

The differences in persistence of the inhibition and of the enhancement of spontaneous emission with an increasing separation of the emitter to the slab can also be understood by analyzing the various guided-mode contributions to the LRDOS of a homogeneous slab. For the frequency a/λ in the gap, no contribution to the LRDOS of the first TE guided mode exists, owing to the TE bandgap. In this frequency range, the only other modes that contribute to the LRDOS in a dielectric slab are the propagating modes and the first TM guided mode. The electric field component parallel to the membrane of the first TM guided mode is zero in the center of the slab but increases monotonically toward the edge of the slab. Indeed, we find excellent agreement of the LRDOS calculated by FDTD for x-oriented dipoles in the membrane, and the sum of

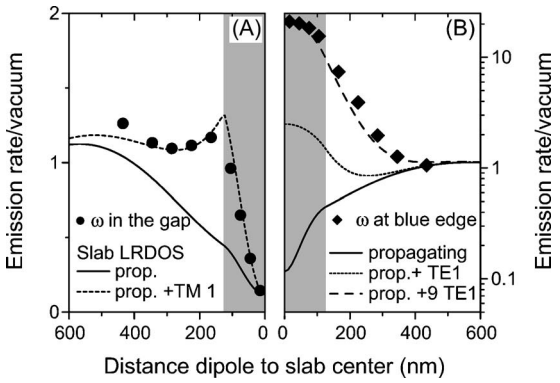

Fig. 10. (A) Symbols, emission rate normalized to vacuum emission rate as a function of the vertical separation between dipole and the center of the membrane for an x-oriented dipole in the central hole of the structure considered in Fig. 4, emitting at a frequency $a/\lambda=0.28$ inside the emission gap. At the inside edge of the membrane and outside the membrane, no trace of inhibition remains. Solid curve, LRDOS contribution of propagating modes for an in-plane oriented dipole in the center of a homogeneous dielectric slab (index 2.8) with the same thickness as the membrane. Dashed curve, same as solid curve, augmented with the contribution of the first TM guided mode to the LRDOS. (B) Symbols, as in (A) but for a frequency $a/\lambda=0.33$ at the blue edge of the gap. Solid curve, propagating-mode LRDOS contribution as in (A). Dotted curve, same as solid curve, augmented with the contribution of the first TE guided mode to the LRDOS of a homogeneous slab. Dashed curve, same as solid curve, augmented with a nine-times-enhanced contribution of the first TE guided mode. The extent of the membrane is shaded in gray in (A) and (B).

LRDOS contributions of propagating modes and the first TM guided mode in a dielectric slab of index 2.8, equal to the volume-averaged refractive index of the photonic crystal. In essence, the range of dipole heights over which inhibition occurs is limited by the parallel electric field profile of the first TM slab mode. In contrast, the enhancement of emission at the blue edge of the gap is due to the photonic-crystal-induced enhanced density of first-order TE guided modes. The emission enhancement as a function of dipole height therefore traces the vertical mode profile of the first TE guided mode. This notion is confirmed by the fact that the enhancement in Fig. 10(b) for a PC membrane can be excellently described as the sum of the propagating mode LRDOS contribution in the effective index slab, augmented by a scaled contribution of the first TE guided mode. Quantitatively, we find that the contribution of the first TE guided mode is enhanced by ~9 times over the contribution of the same mode in a homogeneous slab of the same effective index.

7. ORIENTATIONAL DIPOLE ENSEMBLES

Single quantum emitters that are controlled in position and dipole orientation are required to experimentally confirm the strong dependence on position and polarization of the spontaneous emission rate predicted by the simulations. However, the preparation, manipulation, and detection of high-quantum-efficiency single emitters face many experimental challenges in the near-infrared range, where most photonic crystals operate best. In such experiments, we therefore expect that ensembles of emitters are likely to be used.[53] In this section we evaluate the

emission-rate modification that is observable for a subwavelength-sized orientationally isotropic ensemble of dipoles located in the central air hole of the photonic crystal membrane considered in Figs. 4 and 5. To obtain an angle-averaged modification of the emission rate for an isotropic ensemble of dipole orientations, one often uses a simple average of the LRDOS over three perpendicular dipole orientations.[51] However, because of the angle dependence of the luminescence extraction efficiency[54] η, such a simple average is not suited for reconstructing the ensemble-averaged emission rate modification that is observable with far-field collection optics. The fraction of light emitted into propagating waves instead of the guided mode of the slab depends strongly on dipole orientation. For example, a dramatic increase of the emission extraction efficiency from ~20% for frequencies below the gap to above 80% in the gap occurs for in-plane dipoles. This increase counteracts the reduction in visibility of the emission gap that is naively expected due to the contribution of vertically oriented dipoles.

To assess the changes in the emission dynamics observable in time-resolved fluorescence measurements, we have calculated the LRDOS and η for differently oriented dipoles in the central air hole. We obtained η from the frequency-dependent Poynting vector using on-the-fly discrete Fourier transform of the time-dependent tangential E and H fields on the surface of a box enclosing the crystal structure.[36] To synthesize the observable ensemble-averaged decay dynamics, one needs to average exponential time traces with decay rate set by the LRDOS and weighting factor proportional to η over all possible dipole orientations (described by polar angles ϕ and θ):

$$\langle I(t)\rangle = \frac{I_0}{2\pi}\int_0^{2\pi}\int_0^{\pi/2} \eta(\theta,\phi)\,\gamma(\theta,\phi)\exp[-\gamma(\theta,\phi)t]\sin(\theta)\mathrm{d}\theta\mathrm{d}\phi.$$

Here, time t is in units of the vacuum decay time, and $\gamma(\theta,\phi)$ is the orientation-dependent emission rate normalized to the vacuum emission rate. We have approximated this integral by averaging over more than 300 orientations in 2π solid angle, corresponding to over 25 inequivalent dipole orientations. In general, we obtain strongly nonsingle exponential time traces for the ensemble decay. Figure 11(a) presents the fluorescence decay for three key frequencies $a/\lambda = 0.22, 0.26$, and 0.33 just below, in, and just above the emission gap. At the red edge of the gap the nonexponential decay reveals both an enhanced and an inhibited decay component. For frequencies inside the gap, we predict that the ensemble-averaged decay exhibits a clear slowing of the decay dynamics, while a substantial acceleration is predicted to be observable for frequencies at the blue edge of the gap. The nonexponential nature of the time traces, which for some frequencies is more pronounced than for the three traces shown in Fig. 11(a), requires that experiments be performed with sources for which the decay dynamics in a medium of unmodulated LRDOS is completely understood. Furthermore an analysis method to quantify the overall emission rate modification will be necessary. Here, we consider the first moment $\bar{\tau}$

$$\bar{\tau} = \frac{\int_0^\infty t\langle I(t)\rangle \mathrm{d}t}{\int_0^\infty \langle I(t)\rangle \mathrm{d}t}$$

of the synthesized fluorescence decay to quantify the overall emission rate modification evident in the nonexponential time traces. In Fig. 11(b) we plot the inverse $\bar{\tau}^{-1}$ of the first moment in units of the vacuum decay rate for different emission frequencies. We see that even the dipole orientation-averaged emission will reveal inhibition (enhancement) of the mean lifetime by a factor 3 (5) compared with vacuum.

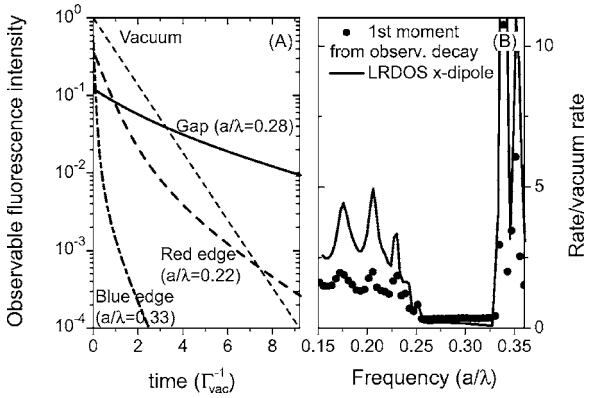

Fig. 11. (A) Simulated fluorescence decay curves (taking extraction efficiency into account) versus time (in units of the vacuum decay time Γ_{vac}^{-1}) for an isotropically oriented ensemble of dipoles in the center of the photonic crystal membrane crystal for three frequencies [below the gap, $a/\lambda = 0.23$ (dash-dotted), in the gap $a/\lambda = 0.28$ (solid), above the gap $a/\lambda = 0.33$ (dashed)]. The dotted line shows the decay of the same ensemble in vacuum. (B) Dots, first moment of simulated decay curves versus emission frequency, in units of the vacuum decay rate. Solid curve, spontaneous emission rate over vacuum rate for a single dipole in the center of the membrane reproduced from Fig. 4.

8. CONCLUSIONS

We have used the 3D FDTD method to systematically investigate the spontaneous emission rate modifications that occur for emitters inside photonic crystal membranes. The spontaneous emission rate depends strongly on dipole position and orientation relative to the crystal lattice. In the central plane of the slab and for in-plane oriented dipoles, the full gap for the first TE guided mode of the vertical structure causes an inhibition of emission by more than seven times compared with vacuum over a large frequency window. In addition, large enhancements of the emission rate occur at the band edges. In the middle of the membrane, vertical index confinement causes the emission rate modifications to be much stronger than in vertically unconfined 2D crystals. The true 3D LRDOS in a photonic crystal membrane mimics the hypothetical 2D LRDOS of a 2D crystal in terms of the frequency bandwidth of the gap, the magnitude of the enhancement (with respect to vacuum) at the band edges, and the variations of the LRDOS spectrum with the lateral position of the dipole in the unit cell. While the LRDOS in the central plane of the membrane can be understood from the 2D band structure, the variation of the

LRDOS with the height of the dipole from the center of the slab can be explained by considering the electric field mode profiles of the lowest few TE and TM guided modes supported by the thin membrane. This is especially relevant for applications that aim at enhancing spontaneous emission. Owing to the vertical extent of the first TE guided mode of the membrane, sizeable emission rate enhancements due to the photonic crystal remain even outside the membrane. For various PC structures of different index contrasts, we have found that the emission rate inside the emission gap reduces exponentially with the system radius to a residual value that can be understood as the LRDOS contribution of modes propagating in air for a homogeneous dielectric slab of proper effective index. We have furthermore presented evidence that the $1/e$ crystal radius associated with the deepening of the emission gap scales inversely with the relative frequency band width of the gap in the 2D dispersion relation. Finally, we have also considered the role of ensemble averaging in experiments that use localized collections of emitters. A realization of such an experiment involves, for instance, a subwavelength ensemble of emitters[53] attached to the end of a sharp glass tip and positioned by using scanning probe techniques, acting as a controllable local probe of the emission modification. Such a subwavelength source averages over an isotropic random distribution of dipole orientations. Despite the presence of dipole orientations that do not match the gap for TE modes, we predict the first moment of the expected nonexponential times traces to show sizeable inhibition and enhancement of the mean emission rate.

ACKNOWLEDGMENTS

We are grateful to Ben Buchler for stimulating discussion. Financial support by EU-projects Development and Analysis of Left-Handed Materials (DALHM), Metamorphose, Phoremost, as well as by the Defense Advanced Research Projects Agency (contract MDA972-01-2-0016)and Ames Laboratory are also acknowledged. This project was performed within the focus program SP1113 of the Deutsche Forschungsgemeinschaft (DFG). F. Koenderink's current address is FOM Institute for Atomic and Molecular Physics, Kruislaan 407 1098 SJ, Amsterdam, The Netherlands. He can be reached by e-mail at F. Koenderink@amolf.nl, and V. Sandoghdar can be reached by e-mail at vahid.sandoghdar@ethz.ch.

REFERENCES

1. K. H. Drexhage, "Influence of a dielectric interface on fluorescence decay time," J. Lumin. **1**, 693–701 (1970).
2. H. Khosravi and R. Loudon, "Vacuum field fluctuations and spontaneous emission in the vicinity of a dielectric surface," Proc. R. Soc. London Ser. A **433**, 337–352 (1991).
3. E. Snoeks, A. Lagendijk, and A. Polman, "Measuring and modifying radiative transitions rate of erbium near an interface," Phys. Rev. Lett. **74**, 2459–2462 (1995).
4. R. M. Amos and W. L. Barnes, "Modification of the spontaneous emission rate of Eu^{3+} ions close to a thin metal mirror," Phys. Rev. B **55**, 7249–7254 (1997).
5. B. C. Buchler, T. Kalkbrenner, C. Hettich, and V. Sandoghdar, "Measuring the quantum efficiency of single radiating dipoles," Phys. Rev. Lett. **95**, 063003:1–4 (2005).
6. P. R. Berman, ed., *Cavity Quantum Electrodynamics* (Academic, 1994).
7. H. Chew, "Radiation and lifetimes of atoms inside dielectric particles," Phys. Rev. A **38**, 3410–3416 (1988).
8. V. V. Klimov, M. Ducloy, and V. S. Letokhov, "Spontaneous emission rate and level shift of an atom inside a dielectric microsphere," J. Mol. Spectrosc. **43** 549–563 (1996).
9. F. L. Kien, N. H. Quang, and K. Hakuta, "Spontaneous emission from an atom inside a dielectric sphere," Opt. Commun. **178**, 151–164 (2000).
10. H. Schniepp and V. Sandoghdar, "Spontaneous emission of europium ions embedded in dielectric nanospheres," Phys. Rev. Lett. **89**, 257403:1-4 (2002).
11. K. J. Vahala, "Optical microcavities," Nature **424**, 839–846 (2003).
12. C. M. Soukoulis, ed., *Photonic Crystals and Light Localization in the 21st Century* (Kluwer Academic, 2001).
13. V. P. Bykov, "Spontaneous emission in a periodic structure," Sov. Phys. JETP **35**, 269–273 (1972).
14. E. Yablonovitch, "Inhibited spontaneous emission in solid-state physics and electronics," Phys. Rev. Lett. **58**, 2059–2062 (1987).
15. C. M. Cornelius and J. P. Dowling, "Modification of Planck blackbody radiation by photonic band-gap structures," Phys. Rev. A **59**, 4736–4746 (1999).
16. M. F. Yanik and S. Fan, "Stopping light all optically," Phys. Rev. A **92**, 083901:1-4 (2005).
17. A. F. Koenderink, L. Bechger, H. P. Schriemer, A. Lagendijk, and W. L. Vos, "Broadband fivefold reduction of vacuum fluctuations probed by dyes in photonic crystals," Phys. Rev. Lett. **88**, 143903:1-4 (2002).
18. P. Lodahl, A. F. van Driel, I. S. Nikolaev, A. Irman, K. Overgaag, D. Vanmaekelbergh, and W. L. Vos, "Controlling the dynamics of spontaneous emission from quantum dots by photonic crystals," Nature **430**, 654–657 (2004).
19. S. P. Ogawa, M. Imada, S. Yoshimoto, M. Okano, S. Noda, "Control of light emission by 3D photonic crystals," Science **305**, 227–229 (2004).
20. Y. Akahane, T. Asano, B. S. Song, S. Noda, "High-Q photonic nanocavity in a two-dimensional photonic crystal," Nature **425**, 944–947 (2003).
21. K. Srinivasan, P. E. Barclay, O. Painter, J. X. Chen, A. Y. Cho, andC. Gmachl, "Experimental demonstration of a high quality factor photonic crystal microcavity," Appl. Phys. Lett. **83**, 1915–1917 (2003).
22. T. Yoshie, A. Scherer, J. Hendickson, G. Khitrova, H. M. Gibbs, G. Rupper, C. Ell, O. B. Shchekin, and D. G. Deppe, "Vacuum Rabi splitting with a single quantum dot in a photonic crystal nanocavity," Nature **432**, 200–203 (2004).
23. A. Kress, F. Hofbauer, N. Reinelt, M. Kaniber, H. J. Krenner, R. Meyer, G. Bohm, and J. J. Finley, "Manipulation of the spontaneous emission dynamics of quantum dots in two-dimensional photonic crystals," Phys. Rev. B **71**, 241304 (2005).
24. D. Englund, D. Fattal, E. Waks, G. Solomon, B. Zhang, T. Nakaoka, Y. Arakawa, Y. Yamamoto, J. Vučković, "Controlling the spontaneous emission rate of single quantum dots in a 2D photonic crystal," Phys. Rev. Lett. **95**, 013904 (2005).
25. M. Fujita, S. Takahashi, Y. Tanaka, T. Asano, and S. Noda, "Simultaneous inhibition and redistribution of spontaneous light emission in photonic crystals," Science **308**, 1296–1298 (2005).
26. K. M. Ho, C. T. Chan, and C. M. Soukoulis, "Existence of a photonic gap in periodic dielectric structures," Phys. Rev. Lett. **65**, 3152–3155 (1990).
27. T. Suzuki and P. K. L. Yu, "Emission power of an electric dipole in the photonic band structure of the fcc lattice," J. Opt. Soc. Am. B **12**, 570–582 (1995).
28. K. Busch and S. John, "Photonic bandgap formation in certain self-organizing systems," Phys. Rev. E **58**, 3896–3908 (1998).
29. K. Busch, N. Vats, S. John, and B. C. Sanders, "Radiating dipoles in photonic crystals," Phys. Rev. E **62**, 4251–4260 (2000).
30. Z. Y. Li, L. L. Lin, and Z. Q. Zhang, "Spontaneous emission

from photonic crystals: full vectorial calculations," Phys. Rev. Lett. **84**, 4341–4344 (2000).
31. R. Z. Wang, X. H. Wang, B. Y. Gu, and G. Z. Yang, "Local density of states in three-dimensional photonic crystals: calculation and enhancement effects," Phys. Rev. B **67**, 155114:1-7 (2003).
32. J.-K. Hwang, H.-Y. Ryu, and Y.-H. Lee, "Spontaneous emission rate of an electric dipole in a general microcavity," Phys. Rev. B **60**, 4688–4695 (1999).
33. Y. Xu, R. K. Lee, and A. Yariv, "Quantum analysis and the classical analysis of spontaneous emission in a microcavity," Phys. Rev. A **61**, 033807:1-13 (2000).
34. R. K. Lee, Y. Xu, A. Yariv, "Modified spontaneous emission from a two-dimensional photonic bandgap crystal slab," J. Opt. Soc. Am. B **17**, 1438–1442 (2000).
35. C. Hermann and O. Hess, "Modified spontaneous emission rate in an inverted-opal structure with complete photonic bandgap," J. Opt. Soc. Am. B **19**, 3013–3018 (2002).
36. A. Taflove and S. C. Hagness, *Computational Electrodynamics: the Finite-Difference Time-Domain Method*,2nd ed. (Artech House, 2000).
37. R. Sprik, B. A. van Tiggelen, and A. Lagendijk, "Optical emission in periodic dielectrics," Europhys. Lett. **35**, 265–270 (1996).
38. I. Daubechies, "Orthonormal bases of compactly supported wavelets," Commun. Pure Appl. Math. **41**, 909–996 (1988).
39. A. F. Koenderink, M. Kafesaki, B. C. Buchler, and V. Sandoghdar, "Controlling the resonance of a photonic crystal microcavity by a near-field probe," Phys. Rev. Lett. **95**, 153904:1–4 (2005).
40. O. Hess, C. Hermann, and A. Klaedtke, "Finite-difference time-domain simulations of photonic crystal defect structures," Phys. Status Solidi A **197**, 605–619 (2003).
41. G. Gilat, "Analysis of methods for calculating spectral properties in solids," J. Comput. Phys. **10**, 432–465 (1972).
42. H. J. Monkhorst and J. D. Pack, "Special points for Brillouin-zone integrations," Phys. Rev. B **13**, 5188–5192 (1976).
43. A. A. Asatryan, K. Busch, R. C. McPhedran, L. C. Botten, C. M. de Sterke, and N. A. Nicorovici, "Two-dimensional Green's function and local density of states in photonic crystals consisting of a finite number of cylinders of infinite length," Phys. Rev. E **63**, 046612:1–4 (2001).
44. D. P. Fussell, R. C. McPhedran, C. M. de Sterke, and A. A. Asatryan, "Three-dimensional local density of states in a finite two-dimensional photonic crystal composed of cylinders," Phys. Rev. E **67**, 045601:1–4 (2003).
45. O. Painter, J. Vučković, and A. Scherer, "Defect modes of a two-dimensional photonic crystal in an optically thin dielectric slab," J. Opt. Soc. Am. B **16**, 275–285 (1999).
46. K. W.-K. Shung and Y. C. Tsai, "Surface effects and band measurements in photonic crystals," Phys. Rev. B **48**, 11265–11269 (1993).
47. Yu. A. Vlasov, M. Deutsch, and D. J. Norris, "Single-domain spectroscopy of self-assembled photonic crystals," Appl. Phys. Lett. **76**, 1627–1629 (2000).
48. J. S. Kole, New methods for the numerical solution of Maxwell's equations, Ph.D. thesis (Rijksuniversiteit Groningen, The Netherlands, 2003), http://www.ub.rug.nl/eldoc/dis/science/j.s.kole/.
49. M. Okano, A. Chutinan, and S. Noda, "Analysis and design of single-defect cavities in a three-dimensional photonic crystal," Phys. Rev. B **66**, 165211:1–6 (2002).
50. W. L. Vos, R. Sprik, A. van Blaaderen, A. Imhof, A. Lagendijk, and G. H. Wegdam, "Strong effects of photonic band structures on the diffraction of colloidal crystals," Phys. Rev. B **53**, 16231–16235 (1996).
51. H. P. Urbach and G. L. J. A. Rikken, "Spontaneous emission from a dielectric slab," Phys. Rev. A **57**, 3913–3930 (1998).
52. A. F. Koenderink, M. Kafesaki, C. M. Soukoulis, and V. Sandoghdar, "Spontaneous emission in the near-field of 2D membrane photonic crystals," Opt. Lett. **30**, 3210–3212 (2005).
53. P. Olk, B. C. Buchler, V. Sandoghdar, N. Gaponik, A. Eychmüller, and A. L. Rogach, "Subwavelength emitters in the near-infrared based on mercury telluride nanocrystals," Appl. Phys. Lett. **84**, 4732–4734 (2004).
54. S. Fan, P. R. Vileneuve, J. D. Joannopoulos, and E. F. Schubert, "High extraction efficiency of epontaneous emission from slabs of photonic crystals," Phys. Rev. Lett. **78**, 3294–3297 (1997).